Acta Neuropathologica (2024) 148:60
https://doi.org/10.1007/s00401-024-02807-w

ORIGINAL PAPER

TMEM106B amyloid filaments in the Biondi bodies of ependymal cells

Bernardino Ghetti[1] · Manuel Schweighauser[2] · Max H. Jacobsen[1] · Derrick Gray[3] · Mehtap Bacioglu[4] · Alexey G. Murzin[2] · Bradley S. Glazier[1] · Taxiarchis Katsinelos[2] · Ruben Vidal[1] · Kathy L. Newell[1] · Sujuan Gao[5] · Holly J. Garringer[1] · Maria Grazia Spillantini[4] · Sjors H. W. Scheres[2] · Michel Goedert[2]

Received: 18 June 2024 / Revised: 11 September 2024 / Accepted: 15 September 2024

Abstract

Biondi bodies are filamentous amyloid inclusions of unknown composition in ependymal cells of the choroid plexuses, ependymal cells lining cerebral ventricles and ependymal cells of the central canal of the spinal cord. Their formation is age-dependent and they are commonly associated with a variety of neurodegenerative conditions, including Alzheimer's disease and Lewy body disorders. Here, we show that Biondi bodies are strongly immunoreactive with TMEM239, an antibody specific for inclusions of transmembrane protein 106B (TMEM106B). Biondi bodies were labelled by both this antibody and the amyloid dye pFTAA. Many Biondi bodies were also labelled for TMEM106B and the lysosomal markers Hexosaminidase A and Cathepsin D. By transmission immuno-electron microscopy, Biondi bodies of choroid plexuses were decorated by TMEM239 and were associated with structures that resembled residual bodies or secondary lysosomes. By electron cryo-microscopy, TMEM106B filaments from Biondi bodies of choroid plexuses were similar (Biondi variant), but not identical, to the fold I that was previously identified in filaments from brain parenchyma.

Keywords Amyloid · Biondi bodies · Electron cryo-microscopy · Ependymal cells · Lysosomes · Transmembrane protein 106B

✉ Bernardino Ghetti
bghetti@iu.edu

Manuel Schweighauser
manuels@mrc-lmb.cam.ac.uk

Max H. Jacobsen
maxhjaco@iu.edu

Derrick Gray
dergray@iu.edu

Mehtap Bacioglu
mb2262@medschl.cam.ac.uk

Alexey G. Murzin
agm@mrc-lmb.cam.ac.uk

Bradley S. Glazier
bsglazie@iu.edu

Taxiarchis Katsinelos
katsinelos@mrc-lmb.cam.ac.uk

Ruben Vidal
rvidal@iu.edu

Kathy L. Newell
klnewell@iu.edu

Sujuan Gao
sgao@iu.edu

Holly J. Garringer
hjgarrin@iu.edu

Maria Grazia Spillantini
mgs11@cam.ac.uk

Sjors H. W. Scheres
scheres@mrc-lmb.cam.ac.uk

Michel Goedert
mg@mrc-lmb.cam.ac.uk

[1] Department of Pathology and Laboratory Medicine, Indiana University School of Medicine, Indianapolis, USA

[2] Medical Research Council Laboratory of Molecular Biology, Cambridge, UK

[3] Center for Electron Microscopy, Indiana University School of Medicine, Indianapolis, USA

[4] Department of Clinical Neurosciences, Cambridge University, Cambridge, UK

[5] Department of Biostatistics, Indiana University School of Medicine, Indianapolis, USA

Published online: 06 November 2024

Introduction

Ependymal cells are postmitotic, originate from radial glia and line choroid plexuses, cerebral ventricles and the central canal of the spinal cord [49, 57]. In choroid plexuses, ependymal cells filter the blood and generate cerebrospinal fluid (CSF), thus regulating the concentration of ions, nutrients and other essential molecules. In the lining of the ventricles and the central canal, multiciliated ependymal cells play an essential role in the propulsion of the CSF.

As a function of age, human ependymal cells are prone to degenerative changes that are most evident as argyrophilic inclusions, which were first described by Del Rio Hortega [14] and subsequently by Biondi [6, 7], after whom they are named (Biondi bodies, Biondi ring tangles and silver rings of Biondi). The amyloid nature of Biondi bodies was established by Divry, who documented the inclusions' birefringency under polarised light in sections stained with Congo red [16]. This conclusion was strengthened by the staining of Biondi bodies using the amyloid dye Thioflavin S [30].

In 1966, Bargmann and Katritsis reported the first electron microscopic pictures of Biondi bodies from choroid plexuses. They demonstrated that the inclusions are made of filaments with a diameter of 10–15 nm [4]. The fine structure of Biondi bodies from the human choroid plexuses was also studied using biopsy material [17, 39]. Electron-dense pigment granules and large lipid droplets were associated with the filamentous structures leading to the suggestion of a lysosomal origin of the inclusions [38, 39]. In addition to their presence in elderly individuals, Biondi bodies have been described to occur concomitantly with Alzheimer disease (AD), Lewy body disorders and other neurodegenerative conditions [12, 34, 53, 55, 63]. Structures resembling Biondi bodies have also been described in the human iris of individuals aged 60 or more and in the choroid plexuses from an aged chimpanzee [40, 47].

Despite this long history, the chemical nature of the amyloid filaments from Biondi bodies has remained unknown. Recently, electron cryo-microscopy (cryo-EM) led to the identification of previously unknown amyloid filaments from human brains that form in an age-related manner and are made of residues 120–254 of the 274 amino acid protein TMEM106B [10, 21, 26, 29, 54]. TMEM106B is a type II transmembrane protein that is highly expressed in neurons and glia and is localised to late endosomal/lysosomal compartments [42]. It remains to be seen if the formation of TMEM106B filaments can influence the development of neurodegenerative diseases. Interestingly, it has been shown that crossing mouse lines that model diseases with TDP-43 or tau inclusions with a line that is knockout for mouse TMEM106B enhances the neurodegenerative phenotypes [18, 22, 23, 64, 71]. It has been proposed that Biondi bodies are the earliest manifestation of cerebral amyloidosis [53]. Immunohistochemical studies have described the presence of TMEM106B inclusions in different cell types and brain regions, including the epithelial cells of the choroid plexuses [43]. However, the link with Biondi bodies was not made.

Here, we show that Biondi bodies are immunoreactive for TMEM106B. By immunoblotting, we identified the 29 kDa band that is diagnostic of TMEM106B filaments and Biondi bodies were labelled by TMEM106B antibodies and the amyloid dye pFTAA. By double labelling immunofluorescence, many Biondi bodies were also labelled for TMEM106B and the lysosomal markers Hexosaminidase A and Cathepsin D. By transmission immunoelectron microscopy of choroid plexuses, filaments were decorated by TMEM106B antibodies and were often associated with structures resembling secondary lysosomes or residual bodies. By cryo-EM, we identified filaments made of residues S120-G254 of TMEM106B that were similar, but not identical, to fold I (Biondi variant).

Materials and methods

Identification of cases

In the Dementia Laboratory at Indiana University, brain sections are routinely stained with Luxol Fast Blue with haematoxylin–eosin (LFB-H&E) to assess the most relevant histological and cellular characteristics of gray and white matter providing important information about the pattern, shape, and structure of cells in a tissue sample. Thioflavin S, Bielschowsky and Bodian silver are used to identify neurofibrillary pathology and Biondi bodies. In this study, we used Thioflavin S staining for the identification of Biondi bodies in the choroid plexuses and the ventricular ependyma. Since calcifications of the choroid plexuses are known to be associated with age, as shown by computerized tomography [67], the histological analysis of choroid plexuses was aided by the use of LFB-H&E to determine the presence of calcifications. The assessment of the presence of Biondi bodies across cases was qualitative. A systematic analysis of the brains and spinal cords from affected individuals, studied neuropathologically between 1992 and 2024, yielded 1126 cases of disease (Table 1). The tissues were collected for past and present research projects; therefore, limitations exist in the representation of racial and ethnic diversity. Data were collected on research subjects' birth sex, race, ethnicity, ages at death, and primary neuropathologic diagnoses (Table 1). In cases of AD, we also used the Braak staging and CERAD scores obtained during the diagnostic process [9, 35].

For statistical analyses, we used two-sample t-tests, Chi-squared tests and analysis of variance (ANOVA). Logistic regression models were used to assess whether differences

Table 1 Cases by primary neuropathological diagnosis

Diagnosis	Total	Birth sex			Age at death				Biondi bodies	
		Female	Male	N/A	Mean	Min	Max	N/A	+	−
Alzheimer disease, Dominantly Inherited	27	14	13	0	51.2	34	76	1	15	12
Alzheimer disease, Sporadic	439	238	198	3	77.4	40	103	3	423	16
Diffuse Lewy body disease	139	41	98	0	78.5	58	95	0	137	2
Multiple system atrophy	6	4	2	0	71.5	52	83	0	6	0
FTLD-Tau, Hereditary	18	9	9	0	58.2	47	65	0	14	4
FTLD-Tau, Sporadic	78	34	44	0	72.3	49	94	0	74	4
FTLD-TDP-43, Hereditary	38	16	22	0	64.3	42	81	0	35	3
FTLD-TDP-43, Sporadic	23	9	14	0	68.1	50	92	0	20	3
Creutzfeldt-Jakob disease, Hereditary	9	5	4	0	61.7	42	85	0	7	2
Creutzfeldt-Jakob disease, Sporadic	115	65	50	0	65.3	33	91	0	93	22
Gerstmann-Sträussler-Scheinker disease	30	12	17	1	53.9	38	73	1	15	15
Amyotrophic lateral sclerosis	14	4	10	0	64.6	49	77	0	14	0
Cerebrovascular disease	27	9	18	0	80.3	52	98	0	26	1
Miscellaneous	29	11	18	0	55.5	5	85	1	18	11
To be determined	134	45	74	15	66.3	14	96	18	108	26
TOTAL	1126	516	591	19	71.73	5	103	24	1005	121

Frontotemporal Lobar Degeneration (*FTLD*), TAR DNA-binding protein 43 (*TDP-43*), Positive (+), Negative (−)

in the incidence of Biondi bodies were related to the ages at death, the birth sex or the primary neuropathological diagnoses. The analyses were carried out using SAS 9.4 software.

Modified Bielschowsky silver

Choroid plexuses and ependymal lining of the lateral ventricles were analyzed from case 1 (Table 2) that was selected from the archival cases that were stained using the modified Bielschowsky silver method [5, 61]. Fixed tissue sections were deparaffinised and hydrated for 3 min, placed in 50 ml 10% silver nitrate for 30 min and washed in water for 3 min. Concentrated ammonium hydroxide was added dropwise, followed by a 15 min incubation. The sections were then washed in 0.1% ammonium hydroxide for 2 min, followed by immersion in developer solution and silver hydroxide solution for 10 min. Next, the sections were washed with 0.1% ammonium hydroxide for 2 min, followed by a 3 min wash in water. They were then placed in 0.2% gold chloride for 5 min and fixed in 5% sodium thiosulfate for 1 min. The sections were washed with water, dehydrated using an increasing alcohol series, put in xylene and mounted.

Bodian silver

Choroid plexuses were analyzed from case 2 (Table 2) selected from archival cases stained using the Bodian silver method carried out according to a published protocol [8, 44]. Sections from paraffin blocks were cut at 8 µm, dried at 60° C for 2 h, deparaffinised in xylene and washed in graded alcohols. The sections were treated with Protargol-S solution for 12–30 h, washed three times with water, treated with hydroquinone/formalin solution for 15 min and washed with water. They were then incubated in 0.2% gold chloride solution for 10–15 min, washed repeatedly with water, incubated with 2% oxalic acid for 2–3 min, washed three times with water and incubated with 5% sodium thiosulfate for 5–10 min. The sections were dehydrated using a graded series of ethanol, cleared with xylene and mounted on glass slides.

Thioflavin S

Choroid plexuses and ependymal lining of the lateral ventricles from cases 1 and 24 (Table 2) and ependymal lining of the central canal of the spinal cord from case 4 (Table 2) were selected from the 1126 archival cases that were stained using Thioflavin S following a described protocol [65]. Fixed tissue sections were deparaffinised and incubated in 1% (w/v) Thioflavin S (Sigma Fine Chemicals) in water for up to 10 min. The sections were then rinsed in 80% (v/v) ethanol (twice for 1 min), followed by water and mounting in aqueous media. Images were acquired using a Leica K5 microscope camera mounted on a Leica THUNDER 3D tissue imager (Leica Microsystems).

Immunohistochemistry

Choroid plexuses and ventricular ependyma from 36 cases including cases 3, 5 and 24 (Table 2) as well as the

Table 2 Subset of Research Cases: 1–24 used for Figures; 1–48 used for TMEM106B Genotype at residue 185

Case	TMEM106B genotype	Birth sex	Age at death (Years)	Primary neuropathological diagnosis	
1	TT	Female	81	Alzheimer disease, Sporadic	1a,1b,1e,1f
2	SS	Female	81	Alzheimer disease, Sporadic	S1a,S1b
3	TT	Female	87	Alzheimer disease, Sporadic	1c,1d,1 g,1 h,2a,2b,2e,2f,3,5a, 9
4	TS	Female	82	Alzheimer disease, Sporadic	S2a,S2b,S2c,S2d
5	TS	Female	96	Alzheimer disease, Sporadic	2 g,2 h
6	TT	Male	67	FTLD-TDP Type A (*GRN*), Hereditary	4c
7	TS	Female	93	Alzheimer disease, Sporadic	4d
8	TS	Female	97	Alzheimer disease, Sporadic	4e,5b,6,8a,S6
9	TT	Female	63	FTLD-Tau, Hereditary	4a
10	TT	Female	67	Alzheimer disease, Dominantly Inherited	4b
11	TT	Male	93	Alzheimer disease, Sporadic	7,S7a,S7b,S8a,S8b
12	TT	Female	70	Alzheimer disease, Sporadic	3
13	TT	Female	68	Alzheimer disease, Sporadic	3
14	TT	Male	61	Alzheimer disease, Sporadic	3,9
15	TS	Male	87	Diffuse Lewy body disease	3
16	TT	Female	91	Alzheimer disease, Sporadic	3
17	TT	Male	70	Alzheimer disease, Sporadic	3
18	TT	Male	57	Alzheimer disease, Sporadic	3
19	TT	Female	70	Alzheimer disease, Sporadic	3
20	TT	Female	60	Alzheimer disease, Sporadic	3,9
21	TS	Female	85	Alzheimer disease, Sporadic	2c,2d
22	TS	Male	78	Alzheimer disease, Sporadic	4f,S5a,S5b
23	TS	Female	71	Alzheimer disease, Sporadic	8b
24	TT	Male	61	Alzheimer disease, Sporadic	S4a,S4b,S4c,S4d
25	TT	Female	50	FTLD-TDP43, Hereditary	N/A
26	TT	Female	75	FTLD-TDP43, Hereditary	N/A
27	TT	Female	42	FTLD-TDP43, Hereditary	N/A
28	TT	Female	59	FTLD-TDP43, Hereditary	N/A
29	TT	Male	34	To be determined	N/A
30	TT	Female	66	FTLD-Tau, Sporadic	N/A
31	TT	Male	91	To be determined	N/A
32	TT	Female	58	Alzheimer disease, Sporadic	N/A
33	TT	Male	63	Alzheimer disease, Sporadic	N/A
34	TT	Male	64	Diffuse Lewy body disease	N/A
35	TS	Male	80	Diffuse Lewy body disease	N/A
36	TS	Male	74	To Be Determined	N/A
37	TS	Female	66	FTLD-TDP43, Hereditary	N/A
38	TS	Male	84	To be determined	N/A
39	TS	Female	43	Alzheimer disease, Hereditary	N/A
40	TS	Male	76	To be determined	N/A
41	TS	Female	80	To be determined	N/A
42	TS	Male	59	Alzheimer disease, Sporadic	N/A
43	TS	Female	54	Alzheimer disease, Hereditary	N/A
44	TS	Male	74	To be determined	N/A
45	SS	Female	82	To be determined	N/A
46	SS	Male	79	To be determined	N/A
47	SS	Male	63	Diffuse Lewy body disease	N/A
48	SS	Female	44	Alzheimer disease, Hereditary	N/A

Frontotemporal Lobar Degeneration (*FTLD*), TAR DNA-binding protein 43 (*TDP-43*), Granulin (*GRN*)

ependyma of the central canal of the spinal cord from case 4 (Table 2) were selected from the archival cases and new sections (8 µm) were used. The following anti-TMEM106B antibodies were used: TMEM239 (1:500), a rabbit polyclonal antibody raised against a synthetic peptide corresponding to residues 239–250 of human TMEM106B [54]; A303-439A (1:200), a mouse monoclonal antibody specific for the N-terminal 50 amino acids of human TMEM106B (Bethyl Laboratories); TMEM263 (1:200), a rabbit polyclonal antibody raised against a synthetic peptide corresponding to residues 263–274 of human TMEM106B [3]. Ependymal cells from the choroid plexuses and ventricular ependyma from 31 of the cases studied were immunopositive with antibody TMEM239. These cases were diagnosed as AD as well as α-synuclein, tau and TDP-43 proteinopathies. A heat-induced epitope retrieval (HIER) with a "Diva Decloaker" solution (BioCare) was used in an antigen retrieval chamber (BioCare). In addition, five cases free of Biondi bodies were used as negative controls. Immunohistochemistry was also carried out using the following monoclonal antibodies: AT8 (Invitrogen) (1:300) specific for phospho-tau (pS202, pT205), NAB228 (Invitrogen) (1:200) specific for Aβ, pS409/410 (Cosmo Bio) (1:1000) specific for phospho-TDP-43, pS129 ASYN (Abcam) (1:800) specific for phospho-α-synuclein, and 3F4 (BioLegend) (1:500) specific for prion protein (PrP). In addition, the following polyclonal antibodies were used: anti-IBA1 (BioCare) (1:200) specific for microglia, and anti-GFAP (BioCare) (1:100) specific for astrocytes. The signal from the antibodies was visualized using avidin–biotin followed by horseradish peroxidase-conjugated streptavidin and the chromogen diaminobenzidine. Sections were counterstained with hematoxylin to show nuclear and cytoplasmic structures. Images were acquired using a Leica DFC7000T camera mounted on a Leica DMR microscope.

Double labelling

Choroid plexuses from cases 6–10 and 22 (Table 2) were selected for TMEM106B and pFTAA double labelling fluorescence. Following overnight incubation with anti-TMEM106B antibodies (TMEM239, A303-439A or TMEM263), the sections were washed in PBS and incubated with Alexa Fluor 647-conjugated secondary antibody (1:250, Invitrogen) and with 3 µM of the amyloid dye pentamer-formyl thiophene acetic acid (pFTAA) [2] for 2 h at room temperature. Nuclei were counterstained with Hoechst dye (2.5 µg/ml, Sigma Fine Chemicals) for 15 min at room temperature. Following washing in PBS, the sections were treated with TrueBlack lipofuscin autofluorescence quencher (Biotum) for 2 min at room temperature. After washing in PBS, they were coverslipped with Fluoromount-G mounting medium (Southern Biotech). Images were captured on a Leica Stellaris 8 confocal microscope and processed using Image J.

Choroid plexuses from case 8 (Table 2) were selected for TMEM106B and Cathepsin D double labelling immunohistochemistry. Following overnight incubation with anti-TMEM106B antibodies (TMEM239, A303-439A or TMEM263) and Cathepsin D antibody (1:300, Santa Cruz), the sections were washed in PBS and incubated with Alexa Fluor conjugated secondary antibodies (1:250, Invitrogen). Nuclei were counterstained with Hoechst dye for 15 min at room temperature. Following washing in PBS, the sections were treated with TrueBlack lipofuscin autofluorescence quencher (Biotum) for 2 min at room temperature. After washing in PBS, they were cover-slipped with Fluoromount-G mounting medium (Southern Biotech). Images were captured on a Leica Stellaris 8 confocal microscope and processed using Image J.

Choroid plexuses from case 3 (Table 2) were selected for TMEM106B and Hexosaminidase A double labelling immunohistochemistry. Paraffin sections were processed from xylene to alcohol to water and then placed into a "Diva Decloaker" solution [BioCare] and run at 110° C for 30 min in the pressure chamber. Slides were cooled and placed in PBS for 5 min. They were then placed into light-resistant chambers for staining. Both antibodies were mixed into one solution of TMEM239 (1:500) and Hexosaminidase A (1:50, R&D Systems) diluted with PBS. The slides were incubated in the chamber for 30 min, rinsed with PBS and incubated for 30 min with the secondary antibodies, which were either rabbit-conjugated Alexa fluor 488 (1:200, Invitrogen) or mouse-conjugated Alexa fluor 594 (1:200, Invitrogen). The slides were then rinsed with PBS and mounted with ProLong gold with DAPI mounting media.

Choroid plexuses from case 22 (Table 2) were used as negative controls. The primary antibody TMEM239 was omitted, to exclude potential artifacts.

Immunoelectron microscopy

Choroid plexuses from ten cases (Table 2) were processed for transmission and immunoelectron microscopy. One mm^3 formalin-fixed tissue blocks were dissected and post-fixed using 2.5% glutaraldehyde and 2% paraformaldehyde overnight at 4° C. The fixatives were then washed away with cacodylate buffer. Additional fixation was carried out using 1% osmium tetroxide and 1.5% potassium ferrocyanide in cacodylate buffer for 1 h at room temperature. Samples were dehydrated using a graded alcohol series, incubated in propylene oxide for 30 min and embedded in EPON resin. The resin-embedded samples were then polymerised at 60° C for 48 h. Ultrathin sections (70 nm) were cut using a diamond knife and placed on 200 mesh nickel grids (EM Sciences FCF200-Ni). The grids were floated on blocking solution

(0.1% BSA-cacodylate in PBS) for 1 h at room temperature, followed by incubation with antibody TMEM239 (1:100) in blocking solution at 4° C overnight. Excess primary antibody was removed with wash buffer (0.01% BSA-cacodylate in PBS). The grids were floated on either 10 nm or 25 nm immunogold gold particles conjugated to goat-anti-rabbit secondary antibodies (EM Sciences 25,109) (1:40) in blocking solution for 2 h at room temperature. Excess secondary antibody was removed with wash buffer, followed by water. The sections were contrasted for 1 min with Uranyless (EM Sciences), washed with water, blotted and dried in a vacuum desiccator for 1 h before imaging. Images were captured on a Tecnai 12 transmission electron microscope operated at 80 kV with a Hamamatsu Orca HR CCD camera.

Genomic analysis

Genomic DNA was extracted from the brains of 48 cases, as described [58] (Table 2). A 470 nucleotide amplicon surrounding coding base 554 of the *TMEM106B* gene (NM_018374.4:c.554G), which is the central base of the codon encoding amino acid 185 (NP_060844.2:p.T185), was amplified by polymerase chain reaction (PCR). The PCR products were screened by agarose gel electrophoresis and sequenced. Oligonucleotides were: 5'-GGTTTAATTTTC TTTGACATTTTGG-3' (forward) and 5'-GGCTCAAGC AGTCCACTGAG-3' (reverse).

Filament extraction

Sarkosyl-insoluble material was extracted, as described [59], from the choroid plexuses of ten cases (numbers 3 and 12–20, Table 2), as well as from the ependymal lining of the lateral ventricles of two of these cases (numbers 3 and 12). Tissues were homogenised in 20 vol (w/v) buffer A (10 mM Tris–HCl, pH 7.4, 0.8 M NaCl, 10% sucrose and 1 mM EGTA), brought to 2% sarkosyl and incubated at 37° C for 30 min. The samples were centrifuged at 10,000 g for 10 min, followed by spinning of the supernatants at 100,000 g for 20 min. Pellets were resuspended in buffer A (700 µl/g tissue) and centrifuged at 5,000 g for 5 min. The supernatants were diluted threefold in buffer B (50 mM Tris–HCl, pH 7.4, 0.15 M NaCl, 10% sucrose and 0.2% sarkosyl), followed by a 30 min spin at 166,000 g. For cryo-EM, the pellets were resuspended in 50 µl/g buffer C (20 mM Tris–HCl, pH 7.4, 100 mM NaCl).

Immunoblotting

Immunoblotting of the sarkosyl-insoluble fractions was carried out as described [54]. Briefly, sarkosyl-insoluble pellets were diluted 1:3 and sonicated for 10 min. Samples were resolved on 4–12% Bis–Tris gels (NuPage) and antibody TMEM239 (1:2,000) was diluted in PBS plus 0.1% Tween-20 and 1% BSA. To enhance the signal, membranes were boiled in PBS for 10 min at 95 °C.

Electron cryo-microscopy

Cryo-EM was carried out using the sarkosyl-insoluble fractions from cases 3, 14, and 20 (Table 2). For cases 14 and 20, we dissected the choroid plexuses; for case 3, we dissected the ventricular ependyma at the level of the temporal horn of the lateral ventricle along with some subependymal parenchymal brain tissue. Cryo-EM grids (Quantifoil 1.2/1.3, 300 mesh) were glow-discharged for 1 min using an Edwards (S150B) sputter coater. Three µl of the sarkosyl-insoluble fractions were applied to glow-discharged grids, followed by blotting with filter paper and plunge-freezing into liquid ethane using a Vitrobot Mark IV (Thermo Fisher Scientific) at 4° C and 100% humidity. Cryo-EM images were acquired on a Titan Krios G2 (Thermo Fisher Scientific) operated at 300 kV and equipped with a Falcon-4 direct electron detector. Images were recorded for 2 s in electron event representation format (EER) [24], with a total dose of 30 electrons/$Å^2$ and a pixel size of 0.824 Å.

Data processing

Datasets were processed in RELION using standard helical reconstruction [25, 31]. Movie frames were gain-corrected, aligned and dose-weighted using RELION's own motion correction programme [72]. Contrast transfer function (CTF) was estimated using CTFFIND4.1 [48]. Filaments were picked manually. Reference-free 2D classification was carried out to select suitable segments for further processing. Initial models for Alzheimer tau and TMEM106B filament folds were generated de novo from 2D class average images using relion_helix_inimodel2d [50]. In addition, the TMEM106B fold I map from AD (EMD-14174 [54]) was used for the refinement of TMEM106B filaments. Three-dimensional auto-refinements were performed in RELION-4.0 and the helical twist and rise were refined using local searches. Bayesian polishing and CTF refinement were used to further improve resolutions [73]. The final maps were sharpened using post-processing procedures in RELION-4.0 and resolution estimates were calculated based on Fourier shell correlation (FSC) between two independently refined half-maps at 0.143 [51]. We used relion_helix_toolbox to impose helical symmetry on the post-processing maps.

Model building and refinement

The atomic model of the TMEM106B fold I structure (PDB:7QVC) was docked manually in the density and

modified using Coot [19]. Model refinement was performed using ISOLDE [13], *Servalcat* [68] and REFMAC5 [36, 37]. The model was validated with MolProbity [11]. Figures were prepared with ChimeraX [45] and PyMOL [60].

Results

Disease cases

Ependymal cells lining the choroid plexuses, the ventricles and the central canal of the spinal cord are present in tissue blocks taken at the level of anatomical areas that face the ventricles or that contain the central canal. A systematic analysis from 1992 to 2024 yielded 1126 cases that were stained using Thioflavin S as part of the diagnostic process (Table 1). The neuropathological diagnoses included dominantly inherited and sporadic AD, diffuse Lewy body disease (DLBD), multiple system atrophy (MSA), dominantly inherited and sporadic forms of frontotemporal lobar degeneration (FTLD) associated with tau or TDP-43 inclusions, dominantly inherited and sporadic Creutzfeldt-Jakob disease (CJD), Gerstmann-Sträussler-Scheinker disease (GSS), amyotrophic lateral sclerosis (ALS) and cerebrovascular disease (CVD), as well as rare neurodegenerative diseases (miscellaneous) and conditions that remain unclassified (to be determined). Of the 1126 cases, 1005 (89.2%) had Biondi bodies in the ependymal lining of the choroid plexuses and/or the ventricles. Biondi bodies were present in Caucasians, Asians, African-Americans and Hispanics.

Upon identifying the cases that had the necessary data elements (neuropathological classification, presence of ependyma, age at death, and birth sex), as well as a suitable number of cases per disease group, 927 cases were used for statistical analyses. At death individuals with Biondi bodies were significantly older than those without [75.2 (SD 10.8) years with Biondi bodies versus 53.3 (SD 10.2) years without Biondi bodies, $p < 0.0001$]. Four individuals with Biondi bodies died at an age (34, 37, 42 and 44 years) earlier than the average. They had the following diseases: familial encephalopathy with neuroserpin inclusion bodies (FENIB) associated with the *SERPINI1* L47P mutation; dominantly inherited AD associated with *PSEN1* mutation M233V; sporadic CJD; dominantly inherited AD associated with *PSEN1* mutation A431E mutation. There were no statistically significant associations between the neuropathological diagnoses and the presence of Biondi bodies when adjusting for age at death and birth sex. Analysis of the data from 329 cases of

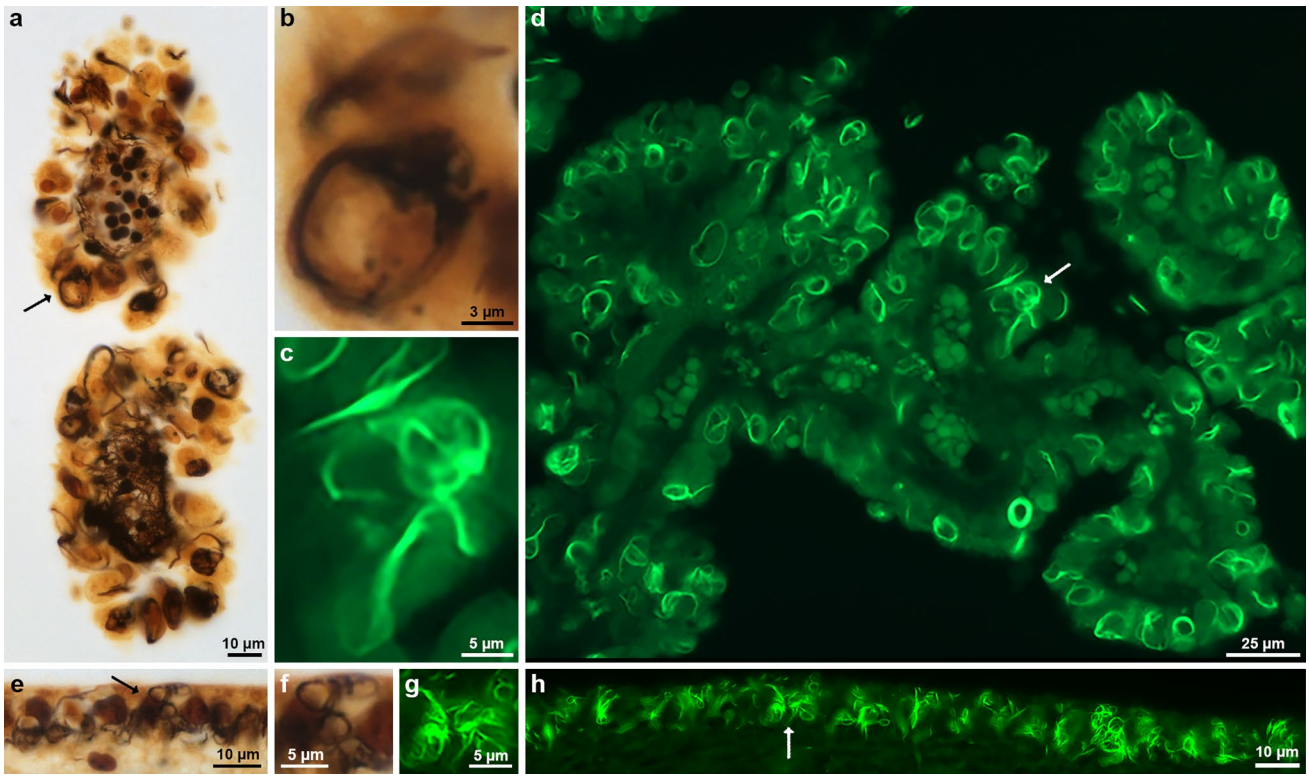

Fig. 1 Histopathology of Biondi bodies using Bielschowsky silver and Thioflavin S. Choroid plexuses (**a**,**d**) and ependymal linings of the lateral ventricle (**e**,**h**) from cases 1 and 3 were stained with modified Bielschowsky silver (**a**,**b**,**e**,**f**) and Thioflavin S (**c**,**d**,**g**,**h**). Biondi bodies are seen in the cytoplasm of ependymal cells as argyrophilic (**a**,**b**,**e**,**f**) or fluorescent (**c**,**d**,**g**,**h**) inclusions. Arrows (**a**,**d**,**e**,**h**) point to Biondi bodies seen at high power in **b**, **c**, **f** and **g**. Scale bars: 10 µm (**a**,**e**,**h**), 3 µm (**b**), 5 µm (**c**,**f**,**g**), and 25 µm (**d**)

AD revealed that there was no difference in Braak staging and CERAD scores between cases with or without Biondi bodies in the choroid plexuses.

We analyzed 67 cases with or without Biondi bodies in the choroid plexuses for the presence of calcifications. The cases were selected to include a wide variety of neuropathological diagnoses, as well as a range of ages at death. Choroid plexuses were examined by light microscopy in sections stained with LFB-H&E and the calcifications were identified for their specific locations, shapes and quantities. We found that approximately 80% of these cases were positive for calcifications, independently of the presence of Biondi bodies.

Biondi bodies can be detected using Thioflavin S, modified Bielschowsky silver and Bodian silver (Fig. 1, Supplementary Fig. 1). We show choroid plexuses and ventricular ependyma from case 1 (Table 2) that were stained with the modified Bielschowsky silver staining technique and Thioflavin S (Fig. 1a,d,e,h). Higher power pictures of ependymal cells (Fig. 1b,c,f,g) illustrate the diversity in shape of Biondi bodies. We also show choroid plexuses from case 2 stained with Bodian silver (Supplementary Fig. 1a,b).

Biondi bodies are immunoreactive for TMEM106B

Antibody TMEM239, which labels TMEM106B inclusions [3, 54], gave strong staining of Biondi bodies in the ependymal cells of the choroid plexuses, as well as in ependymal cells lining the lateral ventricles and the central canal of the spinal cord (Fig. 2a-h; Supplementary Fig. 2a-d). Cases 3 and 5 were used for the choroid plexuses and the linings of the lateral ventricles and case 4 was used for the central canal of the spinal cord (Table 2).

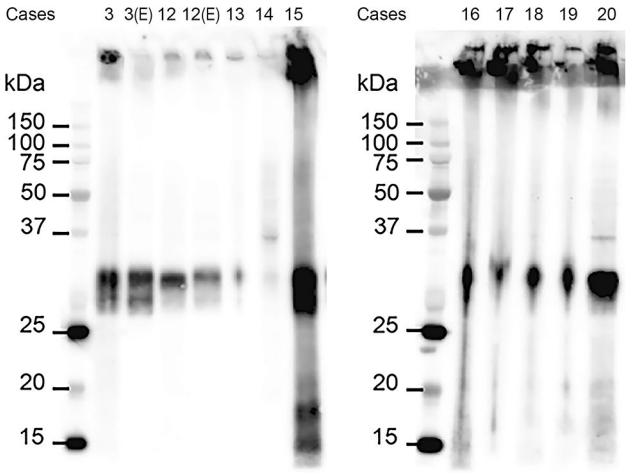

Fig. 3 Immunoblotting of Biondi bodies using antibody TMEM239 and genotyping. Sarkosyl-insoluble extracts from the choroid plexuses of cases 3 and 12–20 and extracts from the ependymal linings of the lateral ventricles from cases 3 and 12 were immunoblotted using antibody TMEM239, which labels TMEM106B inclusions specifically. All extracts showed an immunoreactive band of 29 kDa, diagnostic of the presence of TMEM106B filaments

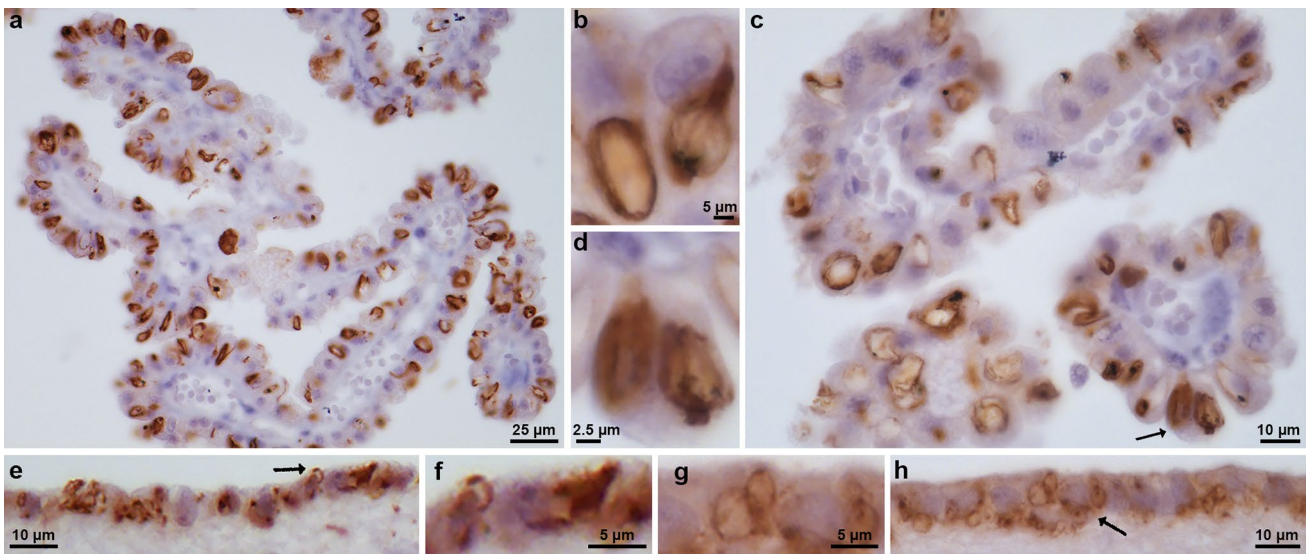

Fig. 2 Immunohistochemistry of Biondi bodies using antibody TMEM239. Choroid plexuses (**a**,**c**) and ependymal linings of the lateral ventricle (**e**,**h**) from cases 3 and 5 were stained using antibody TMEM239, which labels TMEM106B inclusions specifically. Immunoreactive Biondi bodies are seen in (**a**-**h**). Biondi bodies are seen at high power (**b**,**d**,**f**,**g**) and arrows in c, e, and h point to Biondi bodies seen in **d**, **f** and **g**. Scale bars: 25 µm (**a**), 5 µm (**b**,**f**,**g**), 10 µm (**c**,**e**,**h**), and 2.5 µm (**d**)

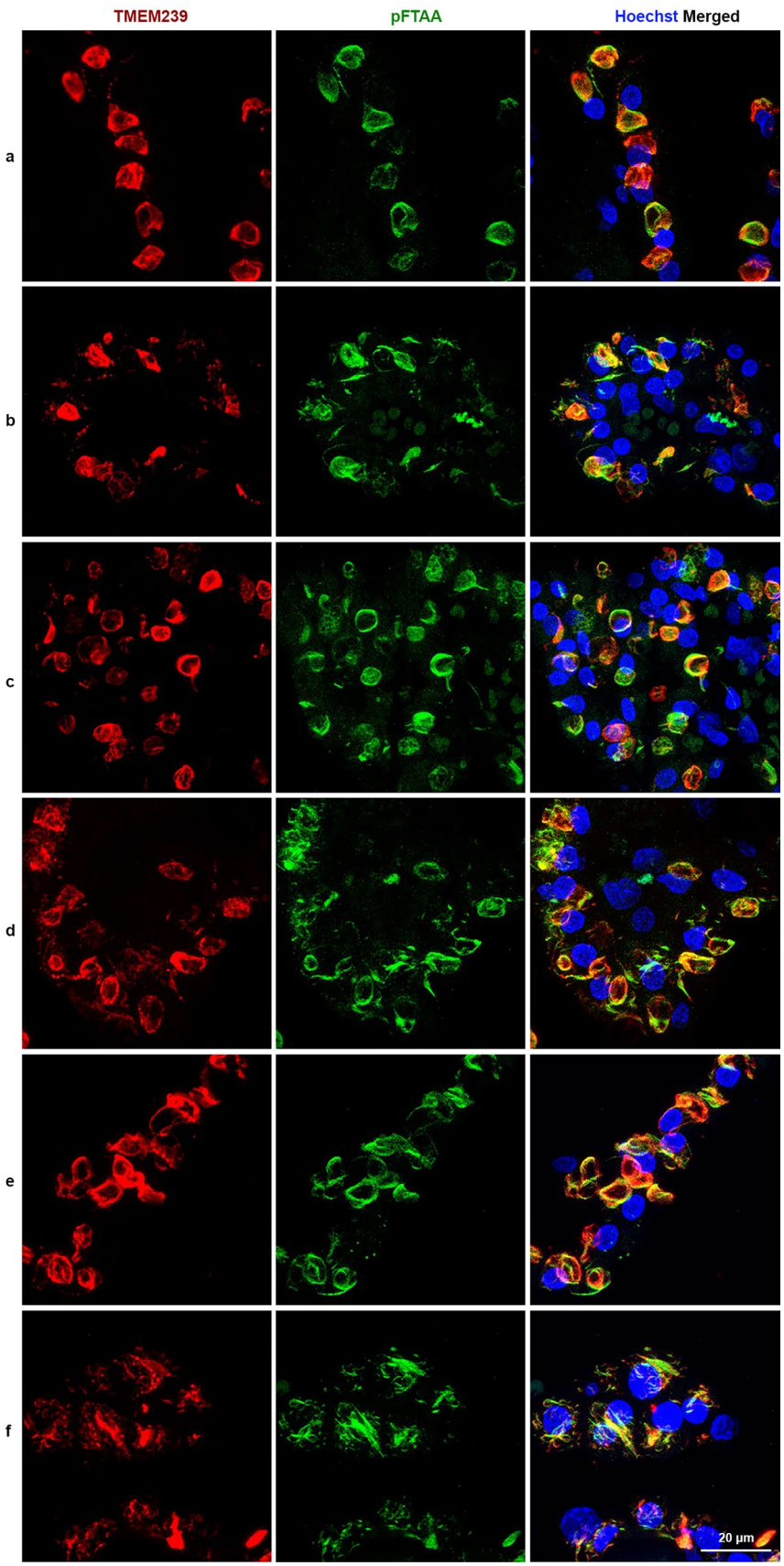

Fig. 4 Double-labelling of choroid plexuses with Biondi bodies using antibody TMEM239 and amyloid dye pFTAA. Choroid plexuses from cases 6–10 and 22. a-f, The panels on the left show single-labelling immunofluorescence by antibody TMEM239 (red); the middle panels show single-labelling fluorescence by the amyloid dye pFTAA (green); the panels on the right show double-labelling by TMEM239 and pFTAA, with the yellow colour appearing when TMEM239 fluorescence and pFTAA fluorescence merge. Nuclei were labelled using Hoechst dye (blue). Scale bar, 20 µm

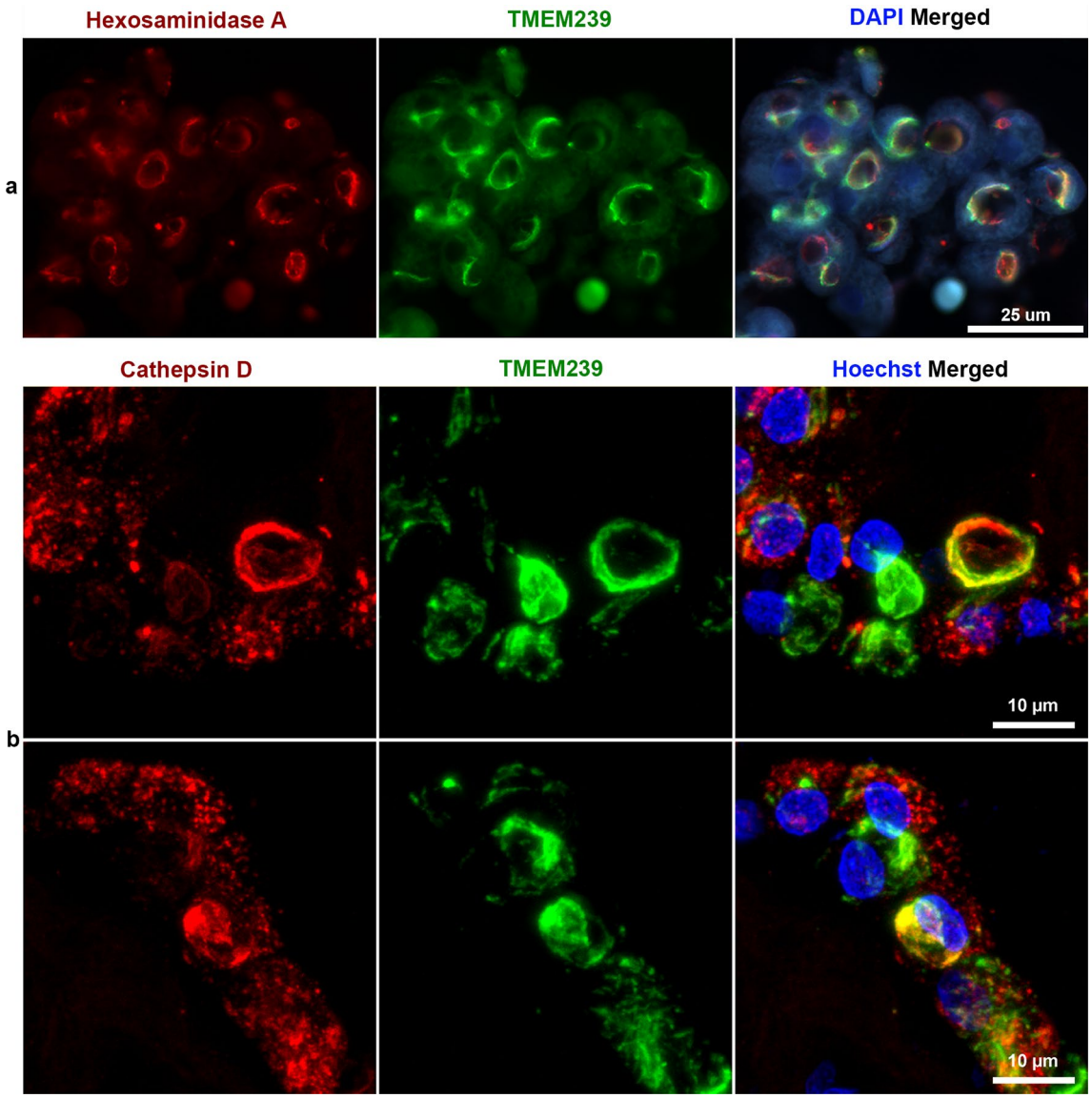

Fig. 5 Immunohistochemistry of Biondi bodies in choroid plexuses using double labelling with an anti-Hexosaminidase A antibody and antibody TMEM239, as well as with an anti-Cathepsin D antibody and antibody TMEM239. Choroid plexuses from cases 3 and 8. **a**, The panel on the left shows single-labelling immunofluorescence by anti-Hexosaminidase A antibody (red); the middle panel shows single-labelling immunofluorescence by antibody TMEM239 (green); the panel on the right shows double-labelling by anti-Hexosaminidase A antibody and antibody TMEM239, with the yellow colour indicating colocalisation. Nuclei were labelled using DAPI (blue). Scale bar, 25 µm. **b**, The panels on the left show single-labelling immunofluorescence by anti-Cathepsin D antibody (red); the middle panels show single-labelling immunofluorescence by antibody TMEM239 (green); the panels on the right show double-labelling, with the yellow colour indicating colocalisation. Nuclei were labelled using Hoechst dye (blue). Scale bar, 10 µm

By immunoblotting, TMEM239 gives a band of 29 kDa that is diagnostic of TMEM106B filaments [54]. We used cases 3 and 12–20 (Table 2) to show the presence of the 29 kDa band in choroid plexuses (Fig. 3); we also used cases 3 and 12 to look for the 29 kDa band in the ependymal lining of the lateral ventricles. Genotyping showed that of the ten cases studied by immunoblotting, nine were homozygous for guanine at position c.554, expressing TMEM106B protein with T185. Only case 15 was heterozygous, thus expressing TMEM106B protein with T185 and S185 (Fig. 3). Labelling with the amyloid dye pFTAA showed co-localisation with TMEM239 staining (Fig. 4 (a-f)). Cases 6–10 and 22 were used (Table 2). In contrast, there was no co-localisation of pFTAA fluorescence and labelling by antibodies specific for

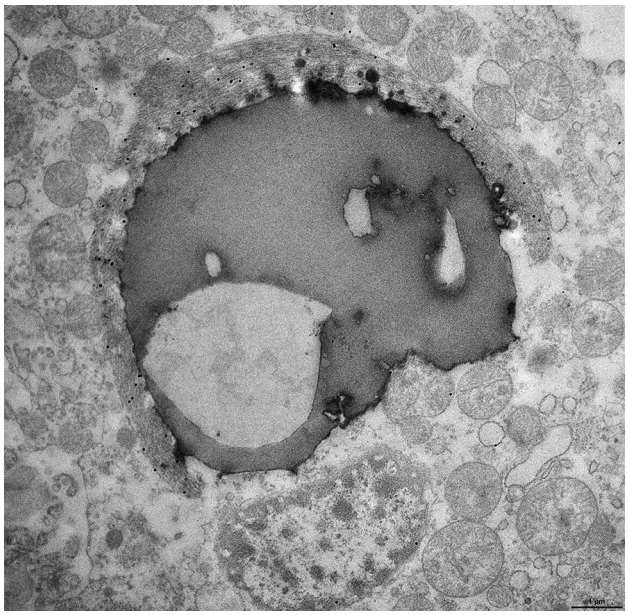

Fig. 6 Immunoelectron microscopy of a Biondi body. Choroid plexuses from case 8 and anti-TMEM106B antibody TMEM239. The cytoplasm of an ependymal cell contains a round body made of osmiophilic and electron-lucent areas that are surrounded by a crescent-shaped bundle of filaments (interpreted as a Biondi body) decorated by gold particles. The round body has the appearance of a secondary lysosome or a residual body. The nucleus of the cell and numerous mitochondria are seen around the inclusion. Scale bar, 1 µm

the N-terminal (A303-439A) and C-terminal (TMEM263) regions of TMEM106B (Supplementary Fig. 3) [3, 54].

Double labelling with the lysosomal markers Hexosaminidase A (Fig. 5a) or Cathepsin D (Fig. 5b) and TMEM239 showed cellular structures labelled with one or the other antibody as well as structures, including many Biondi bodies, that showed co-localisation of both markers. Cases 3 and 8 were used (Table 2). Cases without Biondi bodies did not show TMEM239 staining in the cytoplasm of ependymal cells in choroid plexuses or in the ventricular lining. This was consistent with the lack of fluorescence using Thioflavin S (Supplementary Fig. 4a-d). No immunopositivity was detected in sections labelled in the absence of TMEM239 (Supplementary Fig. 5 a,b). No immunopositivity was detected in any region of the ependymal lining using antibodies specific for proteins related to neurodegeneration: tau (AT8), Aβ (NAB228), TDP-43 (pS409/410), α-synuclein (pS129 ASYN), prion protein (3F4), ionized calcium binding adaptor molecule 1 (IBA1) and glial fibrillary acidic protein (GFAP).

Immunoelectron microscopy of TMEM106B filaments in Biondi bodies

Three cases were selected for Figures (numbers 8, 11, and 23, Table 2). The most frequent finding in ependymal cells of the choroid plexuses was that of large intracytoplasmic inclusions that were composed of two parts: bundles of filaments were closely associated with osmiophilic dense bodies that often contained electron-lucent areas and were reminiscent of secondary lysosomes and residual bodies. Filament bundles were decorated by gold particles following incubation with TMEM239 and secondary antibody; they had a ring, crescent-like or irregular shape and resembled the Biondi bodies seen by light microscopy. Small filament bundles were also present in the cytoplasm, independently of a cellular organelle. The osmiophilic bodies were reminiscent of secondary lysosomes and residual bodies. Figure 6 shows a portion of the cell body of an ependymal cell including the nucleus, numerous mitochondria and a large round structure made of dense osmiophilic material and four electron-lucent or vacuolar areas. The large round structure had the appearance of a secondary lysosome or a residual body that was adherent to a crescent moon-shaped bundle of filaments decorated by gold particles following incubation with antibody TMEM239. Figure 7 shows a Biondi ring made of filaments decorated by gold particles surrounding a large inclusion made of osmiophilic material and an electron-lucent area reminiscent of a residual body. The osmiophilic inclusion, also decorated by gold particles, contains filaments seen in cross-section. The filaments decorated by gold particles measured approximately 10 nm in diameter.

Figure 8a shows a large membrane-bound oval-shaped body containing numerous round osmiophilic bodies and an electron-lucent area. The entire structure is decorated by gold particles and in the upper part, near the membrane, bundles of filaments can also be seen. Figure 8b shows the portion of an ependymal cell in which the main structures are multiple osmiophilic bodies of different dimensions, some were round and large and one had an irregular shape. They were closely connected with a large bundle of decorated filaments intermixed with some of the smaller osmiophilic bodies. Supplementary Fig. 6 shows the cell body of an ependymal cell containing a round body made of osmiophilic material that was closely related to a bundle of filaments decorated by gold particles and was reminiscent of a phrygian cap. The osmiophilic body had the appearance of a secondary lysosome or a residual body. Around the inclusion, the cell nucleus and mitochondria could be seen. Supplementary Fig. 7a shows a large round structure reminiscent of a residual body that was associated with two bundles of filaments decorated by gold particles. In addition, a smaller bundle of filaments, which was also decorated by gold particles, but was not associated with

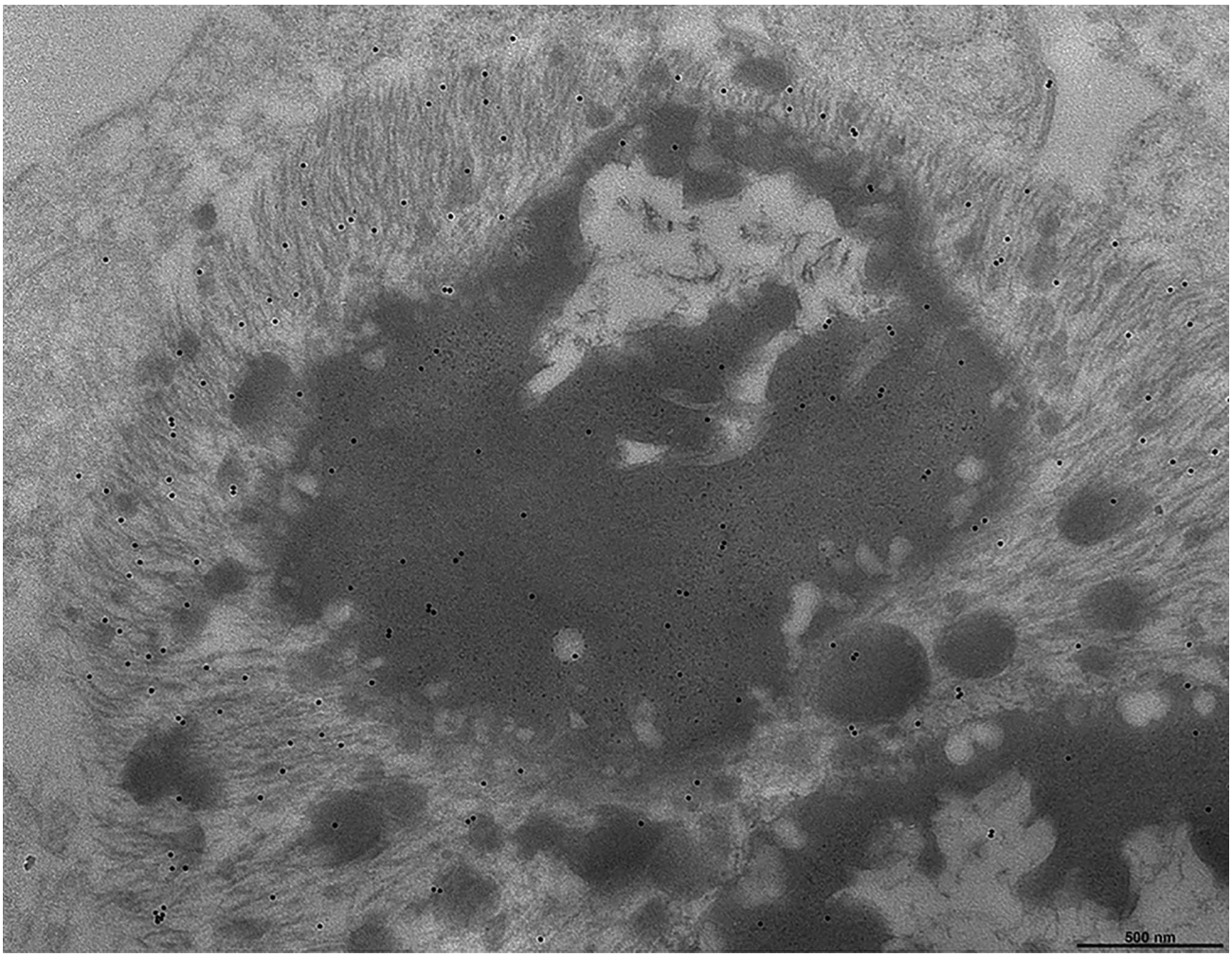

Fig. 7 Immunoelectron microscopy of a Biondi body. Choroid plexuses from case 8 and anti-TMEM106B antibody TMEM239. A Biondi body is shown that consists of a ring of filaments decorated by gold particles surrounding a large osmiophilic inclusion. Note that the large osmiophilic inclusion, also decorated by gold particles, contains what we interpret to be filaments seen in cross-section. Smaller osmiophilic inclusions are intermixed with the filaments. Scale bar, 500 nm

osmiophilic material, can be seen in the lower part. Supplementary Fig. 7b shows a high power view of the bundles of filaments seen on the left of Supplementary Fig. 7a. The filaments can be seen longitudinally; next to them, round structures with an osmiophilic core are also visible that we interpret to be filaments in cross section. The filaments in the bundles decorated by gold particles measured approximately 10 nm in diameter. Supplementary Fig. 8a shows a Biondi ring made of filaments decorated by gold particles that surrounds a large inclusion made of osmiophilic material and an electron-lucent area. Supplementary Fig. 8b shows a bundle of filaments decorated by gold particles that were intermixed with round osmiophilic bodies. All filamentous inclusions in the ependymal cells of the choroid plexuses were decorated by gold particles following incubation with antibody TMEM239.

Cryo-EM structures of TMEM106B filaments from Biondi bodies

The cryo-EM cross-sections of filaments from the sarkosyl-insoluble fractions of the choroid plexuses from individuals with sporadic AD (cases 3, 14 and 20, Table 2) are shown (Fig. 9a). In case 3, the majority of filaments (61%) had the Alzheimer tau fold. This is probably a reflection of the sampling of the ventricular ependyma at the level of the temporal horn of the lateral ventricle, adjacent to the hippocampus. In dissecting the ventricular ependyma, it is unavoidable to include subependymal parenchyma containing neurons.

Ependymal cells were not labelled by the anti-tau antibody AT8, unlike what has been reported [27]. A minority of filaments (8%) from case 14 could not be identified with certainty. In all three cases, the same TMEM106B filament fold was observed that was similar, but not identical, to the

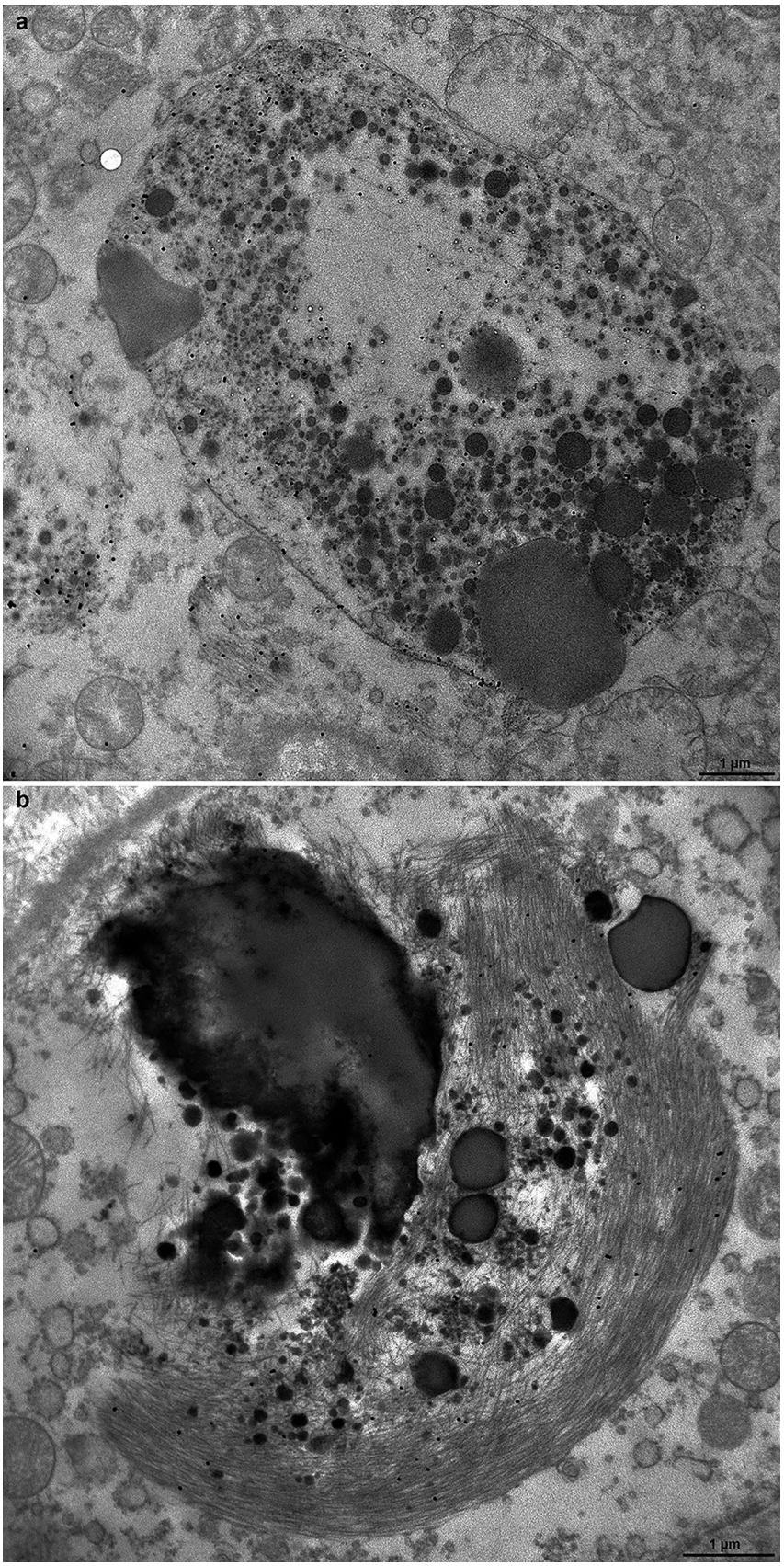

Fig. 8 Immunoelectron microscopy of Biondi bodies. Choroid plexuses from cases 8 and 23 and anti-TMEM106B antibody TMEM239. **a**, A membrane-bound, oval-shaped inclusion is decorated by gold particles and contains round osmiophilic bodies, an electron-lucent area and wisps of filaments. Two bundles of filaments decorated by gold particles are seen outside the membrane-bound inclusion. Scale bar, 1 µm **b**, Multiple osmiophilic bodies of different sizes are intermixed with a large bundle of filaments decorated by gold particles. Scale bar, 1 µm

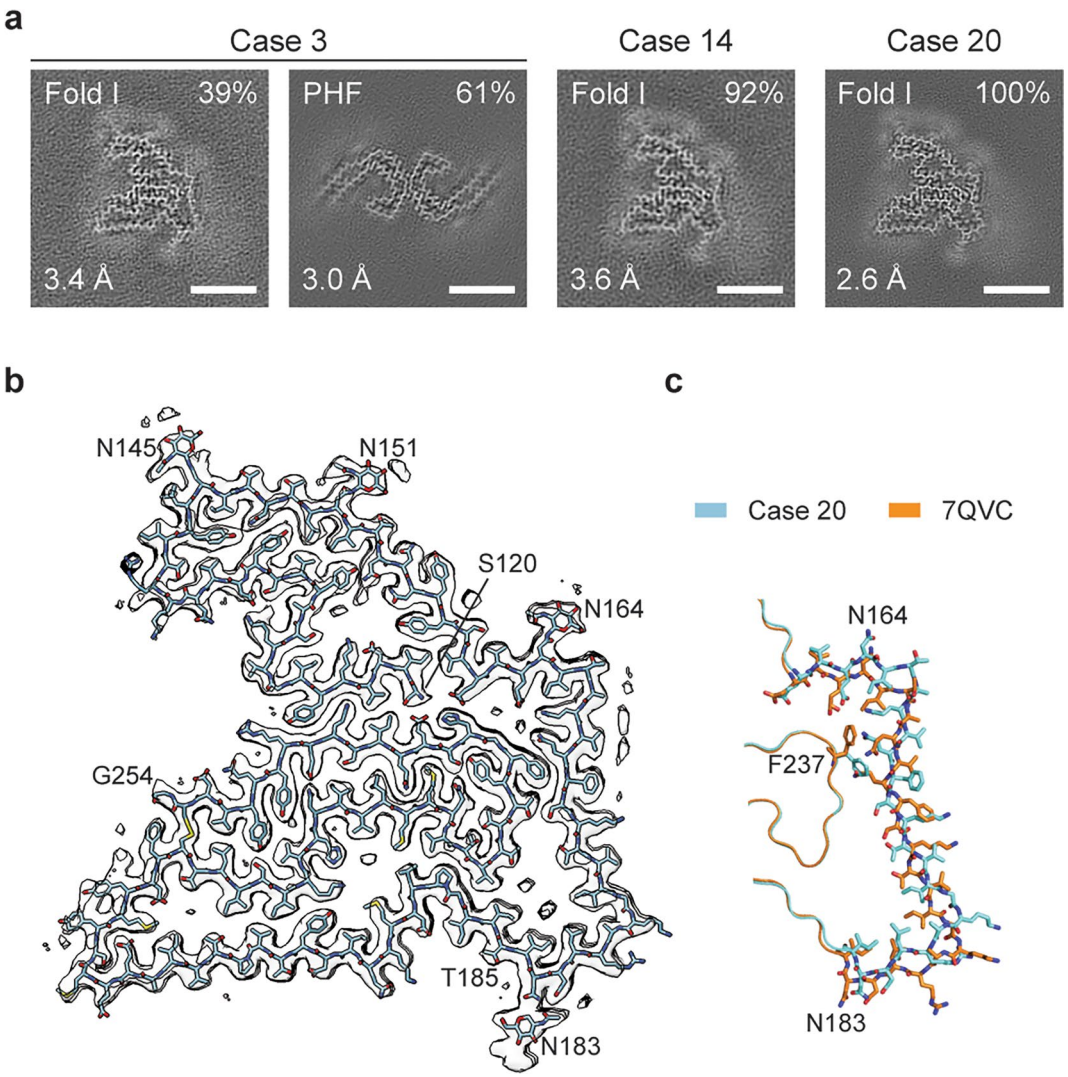

Fig. 9 Cryo-EM structure of TMEM106B filaments from Biondi bodies. Choroid plexuses from cases 3, 14 and 20. **a**, Cross-section through the cryo-EM reconstructions, perpendicular to the helical axis and with a projected thickness of approximately one rung, is shown for the filaments from the sarkosyl-insoluble fractions. The fractions of each filament type and the resolutions are indicated at the top right and bottom left corners, respectively. Scale bars, 5 nm. **b**, Cryo-EM density map (in transparent grey) and atomic model of the TMEM106B filament fold (cyan) from case 20. The amino- and carboxy-terminal residues S120 and G254, glycosylated residues N145, N151, N164 and N183, as well as residue T185 are labelled. c, Comparison of the TMEM106B fold from choroid plexuses of case 20 (cyan) with fold I of TMEM106B filaments from brain parenchyma (orange, PDB:7QVC). The divergent parts of the two folds are shown in sticks. In the rest, both folds are identical. The structures and orientations of their cropped-out parts are as in (**b**)

previously described TMEM106B fold I [54]. The structures of this fold I Biondi variant were determined with resolutions up to 2.6 Å (Fig. 9b). Like the previous folds, it extends from S120-G254 of TMEM106B. However, it differs from the original fold I by a 4 Å shift of an extended segment between glycosylated residues N164 and N183 along its main chain towards the N-terminus and a concomitant rotation of the side chain of F237 in the opposite direction (Fig. 9c). The shift of this segment reduces the size of a large cavity, walled by its C-terminal part, and expands a small cavity near its N-terminus. The larger cavity is surrounded by mostly non-polar side chains and contains two rod-like non-proteinaceous densities, which run parallel to the filament axis. Their size and chemical environment are compatible with the presence of two acyl chains of a lipid molecule. The smaller cavity, which is surrounded by negatively charged and neutral polar groups, contains two rows of small discrete densities that may correspond to ordered solvent molecules, such as ions and water (Fig. 9b). See Supplementary Table 1 and Supplementary Fig. 8 for further details.

Genomic analysis

In 48 cases, DNA sequencing of the *TMEM106B* amplicon surrounding the central nucleotide (NM_018374.4:c.554G) of the codon encoding amino acid 185 (NP_060844.2:p.T185) identified the 3 known genotypes. Twenty-five cases were homozygous for guanine at coding base 554, resulting in both *TMEM106B* alleles producing protein with threonine (TT) at amino acid position 185. Eighteen cases were heterozygous for guanine and cytosine at coding base 554, leading to the production of TMEM106B protein with both threonine and serine residues (TS) at position 185. Five cases were homozygous for cytosine at coding base 554, resulting in both *TMEM106B* alleles producing protein with serine residues (SS) at position 185.

Discussion

Biondi bodies are filamentous amyloid inclusions in the ependymal cells of the choroid plexuses, the lining of the cerebral ventricles and the central canal of the spinal cord. We examined 1126 cases, with a mean age at death of 75 years. Previous studies have shown that the incidence of Biondi bodies increases with age; similarly, the incidence of calcifications in choroid plexuses increases with age [20, 56, 67]. We found that 89% of cases had Biondi bodies and were significantly older than those without Biondi bodies. Calcifications of the choroid plexuses were seen in 80% of a subset of cases, consistent with a previous report [67]. Additional statistical analysis did not find any correlations between the presence of Biondi bodies and a given neurodegenerative disease. Individuals with AD represented the largest segment of the cohort. Disease severity, as measured by Braak staging and CERAD scores, was compared to the presence or absence of Biondi bodies to determine whether there was any relationship between these elements, but none was found.

Here, we report for the first time the presence of TMEM106B in Biondi bodies and establish a direct link between Biondi bodies and filamentous TMEM106B. We also show by cryo-EM that the TMEM106B filaments from Biondi bodies are similar, but not identical, to the TMEM106B filaments with fold I that have been described for filaments from brain parenchyma of aged controls and from individuals with a variety of neurodegenerative diseases [10, 21, 26, 29, 54]. Considering that TMEM106B filaments have been shown to be present in neurons and glia [26, 42, 54], our method of dissection was specifically targeted to the ependymal cells of the choroid plexuses and the ventricular lining. The presence of filaments with the Alzheimer tau fold in addition to the Biondi variant of assembled TMEM106B in one case was probably the result of the presence of brain parenchyma adjacent to the ependymal lining. In previous reports, TMEM106B filaments studied using cryo-EM were obtained from neocortex, caudate nuclei and non-specified brain areas [10, 21, 26, 29, 54]. Since the caudate nuclei face the lateral ventricles, ependymal cells may have been present in some of those samples.

Biondi bodies were strongly labelled by antibody TMEM239, which is specific for TMEM106B filaments, and by the amyloid dye pFTAA, but not by anti-TMEM106B antibodies A303-439A and TMEM263, whose epitopes are in the N- and C-terminal regions, respectively. These results are similar to those reported for TMEM106B inclusions from brain parenchyma [3]. Filaments made of residues S120-G254 of TMEM106B may thus be the major components of the amyloid inclusions of Biondi bodies.

The 31 cases for which TMEM106B immunopositivity of Biondi bodies in the choroid plexuses and ventricular ependyma was seen had also TMEM106B inclusions in brain parenchyma (data not shown). It remains to be seen if this is generally the case. Biondi bodies containing TMEM106B filaments and parenchymal inclusions of TMEM106B both increase in number with age in neurologically normal individuals [54, 63]. Whether the formation of TMEM106B inclusions can influence the development of neurodegenerative disease is not known.

TMEM106B is a type II transmembrane protein of late endosomes and lysosomes. Ependymal cells of the human choroid plexuses undergo conspicuous changes associated with aging, including an increase in lipid droplets in the cytoplasm, giving it a vacuolated appearance [1]. By immunoelectron microscopy of choroid plexuses, TMEM106B filaments were frequently found in association with vacuoles within osmiophilic bodies that had the appearance of secondary lysosomes and residual bodies. Similar findings have also been obtained in brain parenchyma with TMEM106B inclusions [3].

In view of the fact that residual bodies are a product of lysosomal digestion, our findings suggest that TMEM106B may be able to assemble into filaments in close association with lysosomal components. Thus, to investigate a possible relationship between lysosomes and Biondi bodies that are made of TMEM106B filaments, we used antibodies to Hexosaminidase A and Cathepsin D, as markers of mature lysosomes along with antibody TMEM239 [41, 46, 66]. Using double labelling immunohistochemistry, we found that many Biondi bodies labelled by TMEM239 were also labelled by a lysosomal marker, either Hexosaminidase A or Cathepsin D, and that a colocalization of TMEM106B and lysosomal markers could be seen. These data suggest that the Biondi body may represent an intracytoplasmic inclusion resulting from the decay of lysosomal cellular elements as consequence of the involution of ependymal cells.

Astrocytes are the major cell type with TMEM106B inclusions in the brain [3, 21, 28, 32, 43, 69]. Ependymal cells are derived from radial glia and share several cytological features with astrocytes [57]. In the brain parenchyma, TMEM106B filaments have been found to have one of three folds, with fold I being the most prevalent [10, 21, 26, 29, 54]. By cryo-EM, TMEM106B filaments from ependymal cells with Biondi bodies present a new variant of fold I. It may be the result of the different cellular milieu in ependymal cells when compared to brain cells. It remains to be seen if this Biondi variant can also form cofactor-mediated dimeric filaments, as was the case of the original fold I [54]. The relevant cofactors may not be present in ependymal cells. However, future studies of choroid plexuses are needed to answer this question. The cases analyzed by cryo-EM are all homozygous for the T185 variant. Considering that the cases in our cohort that were analyzed genetically revealed T homozygosity (TT) in over 50%, a prospective study by cryo-EM will be needed to establish whether structural differences may exist among TMEM106B filaments of Biondi bodies associated with S homozygosity (SS) or TS heterozygosity (TS).

There are several types of ependymal cells according to different localizations, morphologies, surface markers and functions [15]. In spite of this heterogeneity, they all appear to be able to form Biondi bodies, whether in the choroid plexuses, the lining of the ventricles or the central canal. Ependymal cells are central to the production of CSF, 90% of which is produced by those in the choroid plexuses [49]. CSF production is decreased in elderly individuals [33]. It remains to be established if this decrease is related to the presence of Biondi bodies and if the composition of the CSF may be affected. It will also be interesting to look for the presence of TMEM106B aggregates in CSF. The secretion of Biondi bodies into the CSF has been reported [38].

Flortaucipir and PBB3 are two positron emission tomography (PET) ligands that are being used for the imaging of tau pathology in patients with AD. Flortaucipir has been reported to give off-target binding in the choroid plexuses [52, 62], whereas PBB3 has been shown to bind to TMEM106B [70]. Thus, our finding that TMEM106B is a major component of the amyloid filaments of Biondi bodies suggests that flortaucipir may also bind to TMEM106B and that both PET ligands may be useful for the study of ependymal cells during ageing.

This study provides new perspectives of the alterations of the ependymal cells in age-related diseases with implications of the ependymal function in the production of CSF and other aspects of cerebral homeostasis and may have profound clinical relevance.

Supplementary Information The online version contains supplementary material available at https://doi.org/10.1007/s00401-024-02807-w.

Acknowledgements We are grateful to the patients' families for donating brain tissues. We thank R. Richardson, N. Maynard and K. Cox for technical support. This work was supported by the Center for Electron Microscopy of the Indiana University School of Medicine. It was also supported by the Electron Microscopy Facility of the MRC Laboratory of Molecular Biology. We thank J. Grimmett, T. Darling and I. Clayson for help with high-performance computing

Author contributions B.G., M.H.J., and B.S.G. identified disease cases; B.G. and K.L.N. carried out neuropathology; B.G., M.H.J., K.L.N., M.B. and M.G.S. performed immunohistochemistry; H.J.G. and R.V. carried out genetic analysis. B.G. and D.G. carried immuno-electron microscopy; S.G. carried out data analysis and statistics; M.S. and T.K. prepared filaments and performed immunoblots; M.S. carried out cryo-EM data acquisition; M.S. and A.G.M. carried out structure determination. B.G., S.H.W.S. and M.G. supervised the project and all authors contributed to the writing of the manuscript.

Funding This work was supported by the US National Institutes of Health (grants P30-AG010133 to B.G., P30-AG072976 to B.G., R01-AG075802 to B.G., R01-NS110437 to B.G. and R.V., and R01-NS137469 to K.L.N.), the Jay C. and Lucile L. Kahn Alzheimer Disease Research and Education Professorship to K.L.N., Department of Pathology and Laboratory Medicine, Indiana University School of Medicine, the Cambridge Biomedical Research Centre (NIHR 203312, to M.G.S.) and the UK Medical Research Council (MC_UP_A025-1013 to S.H.W.S. and MC_U105184291 to M.G.).

Data availability The cryo-EM map of the TMEM106B filament from case 12 has been deposited in the Electron Microscopy Data Bank (EMDB) with accession number EMD-50587. The corresponding refined atomic model has been deposited in the Protein Data Bank (PDB) under accession number 9FNB. Please address requests for materials to the corresponding author.

References

1. Adams RD, Oksche A, and Haymaker W "Meninges, choroid plexuses, ependyma and their reactions. (1982) Part 2: Age-related changes and pathology." Histology and Histopathology of the Nervous System. Springfield, IL: Charles C. Thomas: 641–713.
2. Åslund A, Sigurdson CJ, Klingstedt T, Gratwohl S, Bolmont T, Dickstein DL et al (2009) Novel pentameric thiophene derivatives for *in vitro* and *in vivo* imaging of a plethora of protein aggregates in cerebral amyloidoses. ACS Chem Biol 4:673–683
3. Bacioglu M, Schweighauser M, Gray D, Lövestam S, Katsinelos A, Quaegebeur A et al (2024) Cleaved TMEM106B forms

amyloid aggregates in central and peripheral nervous systems. Acta Neuropathol Commun 12:99
4. Bargmann W, Katritsis E (1966) Über die sogenannten Filamente und das Pigment im Plexus chorioideus des Menschen. Z Zellforsch 75:366–370
5. Bielschowsky M (1909) Eine Modifikation meines Silberimprägnationsverfahrens zur Darstellung der Neurofibrillen. J Psychol Neurol 12:135
6. Biondi G (1933) Ein neuer histologischer Befund am Epithel des Plexus chorioideus. Z ges Neurol Psychiat 144:161–165
7. Biondi G (1934) Zur Histopathologie des menschlichen Plexus chorioideus und des Ependyms. Arch Psychiatr Nervenkrankh 101:66–728
8. Bodian D (1936) A new method for staining nerve fibers and nerve endings in mounted paraffin sections. Anat Rec 65:89–97
9. Braak H, Braak E (1991) Neuropathological stageing of Alzheimer-related changes. Acta Neuropathol 82:239–259
10. Chang A, Xiang X, Wang J, Lee C, Arakhamia T, Simjanoska M et al (2022) Homotypic fibrillization of TMEM106B across diverse neurodegenerative diseases. Cell 185:1346–1355
11. Chen VB, Arendall WB, Head JJ, Keedy DA, Immormino RM, Kaprai GI et al (2010) MolProbity: all-atom structure validation for macromolecular crystallography. Acta Crystallogr D 66:12–21
12. Cottrell DA, Ince PG, Wardell TM, Turnbull DM, Johnson MA (2001) Accelerated ageing changes in the choroid plexus of a case with multiple mitochondrial DNA deletions. Neuropathol Appl Neurobiol 27:206–214
13. Croll TI (2018) ISOLDE: a physically realistic environment for model building into low-resolution electron density map. Acta Crystallogr D 74:519–530
14. Del Rio Hortega P (1918) Noticia de un nuevo y fácil método para la coloración de la neuroglia y del tejido conjuntivo. Trab Lab Invest Biol Univ Madrid 15:367–378
15. Deng S, Gan L, Liu C, Xu T, Zhou S, Guo Y et al (2023) Roles of ependymal cells in the physiology and pathology of the central nervous system. Aging Dis 14:468–483
16. Divry P (1955) De la nature des formations argentophiles des plexus choroïdes. Acta Neurol Belg 55:282–283
17. Dohrmann GJ, Bucy PC (1970) Human choroid plexus: a light and electron microscopic study. J Neurosurg 33:506–516
18. Edwards GA, Wood CA, He Y, Nguyen Q, Kim PJ, Gomez-Gutierrez R et al (2024) TMEM106B coding variant is protective and deletion detrimental in a mouse model of tauopathy. Acta Neuropathol 147:61
19. Emsley P, Lohkamp B, Scott WG, Cowtan K (2010) Features and development of Coot. Acta Crystallogr D 66:486–501
20. Eriksson L, Westermark P (1986) Intracellular neurofibrillary tangle-like aggregations. A constantly present amyloid alteration in the aging choroid plexus. Am J Pathol 125:124–129
21. Fan Y, Zhao Q, Xia W, Tao Y, Yu W, Chen M et al (2022) Generic amyloid formation of TMEM106B in a patient with Parkinson's disease dementia and normal elders. Cell Res 32:585–588
22. Feng T, Mai S, Roscoe JM, Shen RR, Ullah M, Zhang J et al (2020) Loss of TMEM106B and PRGN leads to severe lysosomal abnormalities and neurodegeneration in mice. EMBO Rep 21:e50219
23. Feng T, Du H, Yang C, Wang Y, Hu F (2024) Loss of TMEM106B exacerbates tau pathology and neurodegeneration in PS19 mice. Acta Neuropathol 147:62
24. Guo H, Franken E, Deng Y, Benlekbir S, Lezcano GS, Janssen B et al (2020) Electron-event representation data enable efficient cryo-EM file storage with full preservation of spatial and temporal resolution. IUCrJ 7:860–869
25. He S, Scheres SHW (2017) Helical reconstruction in RELION. J Struct Biol 193:163–176
26. Hoq MR, Bharath SR, Hallinan GI, Fernandez A, Vago FS, Ozcan KA et al (2023) Cross-β helical filaments of tau and TMEM106B in gray and white matter of multiple system tauopathy with presenile dementia. Acta Neuropathol 145:707–710
27. Ikonomovic MD, Abrahamson EE, Price JC, Mathis CA, Klunk WE (2016) Positron emission tomography retention in choroid plexus: More than "off target" binding. Ann Neurol 80:307–308
28. Ishikawa R, Yamazaki Y, Nakamori M, Takahashi T, Maruyama H (2023) Antibody recognizing residues 188–211 of TMEM106B exhibit immunohistochemical reactivity with the TMEM106B C-terminal fragment. Front Neurosci 17:1250547
29. Jiang YX, Cao Q, Sawaya MR, Abskharon R, Ge OP, DeTure M et al (2022) Amyloid fibrils in FTLD-TDP are composed of TMEM106B and not TDP-43. Nature 605:304–309
30. Kelényi G (1967) Thioflavin S fluorescent and Congo red anisotropic stainings in the histologic demonstration of amyloid. Acta Neuropathol 7:336–348
31. Kimanius D, Dong L, Sharov G, Nakane T, Scheres SHW (2021) New tools for automated cryo-EM single-particle analysis in RELION-4.0. Biochem J 478:4169–4185
32. Marks JD, Ayuso VE, Carlomagno Y, Yue M, Todd TW, Hao Y et al (2024) TMEM106B core deposition associates with TDP-43 pathology and is increased in risk SNP carriers for frontotemporal dementia. Sci Transl Med 16(730):eadf9735
33. May C, Kaye JA, Atack JR, Schapiro MB, Friedland RP, Rapoport SI (1990) Cerebrospinal fluid production is reduced in healthy aging. Neurology 40:500–503
34. Miklossy J, Kraftsik R, Pillevuit O, Lepori D, Genton C, Bosman FT (1998) Curly fiber and tangle-like inclusions in the ependyma and choroid plexus – a pathogenetic relationship with the cortical Alzheimer-type changes? J Neuropathol Exp Neurol 57:1202–1212
35. Mirra SS, Heyman A, McKeel D, Sumi SM, Crain BJ, Brownlee LM et al (1991) The Consortium to Establish a Registry for Alzheimer's Disease (CERAD). Part II. Standardization of the neuropathologic assessment of Alzheimer's disease. Neurology 41:479–486
36. Murshudov GN, Vagin AA, Dodson EJ (1997) Refinement of macromolecular structures by the maximum-likelihood method. Acta Crystallogr D 53:240–255
37. Murshudov GN, Skubák P, Lebedev AA, Pannu NS, Steiner RA, Nicholls RA et al (2011) REFMAC5 for the refinement of macromolecular crystal structures. Acta Crystallogr D 67:255–267
38. Oksche A, Kirschstein H (1972) Entstehung und Ultrastruktur der Biondi-Körper in den Plexus chorioidei des Menschem (Biopsiematerial). Z Zellforsch 124:320–341
39. Oksche A, Vaupel-von Harnack M (1969) Elektronenmikroskopische Studien über Altersveränderungen (Filamente) der Plexus chorioidei des Menschen (Biopsiematerial). Z Zellforsch 93:1–29
40. Oksche A, Liesner R, Tigges J, Tigges M (1984) Intraepithelial inclusions resembling Biondi bodies in the choroid plexus of an aged chimpanzee. Cell Tissue Res 235:467–469
41. Pastores GM, Kolodny EH (2003) Lysosomal storage disorders. In: Aminoff MJ, Daroff RB (eds) Encyclopedia of the Neurological Sciences. Academic Press, pp 846–855
42. Perneel J, Rademakers R (2022) Identification of TMEM106B amyloid fibrils provides an updated view of TMEM106B biology in health and disease. Acta Neuropathol 144:807–819
43. Perneel J, Neumann M, Heeman B, Cheung S, Van den Broeck M, Wynants S et al (2023) Accumulation of TMEM106B C-terminal fragments in neurodegenerative disease and aging. Acta Neuropathol 145:285–302
44. Persuy P, Défossez A, Delacourte A, Tramu G, Bouchez B, Arnott G (1985) Anti-PHF antibodies; an immunohistochemical marker of the lesions of the Alzheimer's disease. Characterization and

comparison with Bodian's silver impregnation. Virchows Arch Pathol Anat 407:13–23
45. Pettersen EF, Goddard TD, Huang CC, Meng EC, Couch GS, Croll TI et al (2011) Chimera X: structure visualisation for researchers, editors and developers. Protein Sci 30:70–82
46. Press EM, Porter RR, Cebra J (1960) The isolation and properties of a proteolytic enzyme, cathepsin D, from bovine spleen. Biochem J 74:501–514
47. Ringvold A (1974) Biondi-like cell inclusions in the human iris. Acta Ophthalmol 52:541–550
48. Rohou A, Grigorieff N (2015) CTFFIND4: fast and accurate defocus estimation from electron micrographs. J Struct Biol 192:216–221
49. Saunders NR, Dzegielewaska KM, Fame RM, Lehtinen MK, Liddelow SA (2023) The choroid plexus: a missing link in our understanding of brain development and function. Physiol Rev 103:919–956
50. Scheres SHW (2020) Amyloid structure determination in RELION-3.1. Acta Crystallogr D 76:94–101
51. Scheres SHW, Chen S (2012) Prevention of overfitting in cryo-EM structure determination. Nature Meth 9:8453–8454
52. Schöll M, Lockhart SN, Schonhaut DR, O'Neil JP, Janabi M, Ossenkoppele R et al (2016) PET imaging of tau deposition in the aging human brain. Neuron 89:971–982
53. Schwartz P (1970) Amyloidosis: cause and manifestation of senile deterioration. Charles C. Thomas Publisher, Springfield, IL
54. Schweighauser M, Arseni D, Bacioglu M, Huang M, Lövestam S, Shi Y et al (2022) Age-dependent formation of TMEM106B amyloid filaments in human brains. Nature 605:310–314
55. Serot JM, Béné MC, Faure GC (2003) Choroid plexus, aging of the brain, and Alzheimer's disease. Front Biosci 8:s515–s521
56. Shuangshoti S, Netsky MG (1970) Human choroid plexus: morphologic and histochemical alterations with age. Am J Anat 128:73–95
57. Spassky N, Merkle FT, Flames N, Tramontin AD, Garcia-Verdugo JM, Alvarez-Buylla A (2005) Adult ependymal cells are postmitotic and are derived from radial glial cells during embryogenesis. J Neurosci 25:10–18
58. Spina S, Farlow MR, Unverzagt KW, Kareken DA, Murrell JR, Fraser G et al (2008) The tauopathy associated with mutation +3 in intron 10 of Tau: Characterization of the MSTD family. Brain 131:72–89
59. Tarutani A, Arai T, Murayama S, Hisanaga SI, Hasegawa M (2018) Potent prion-like behaviors of pathogenic α-synuclein and evaluation of inactivation methods. Acta Neuropathol Commun 6:29
60. The PyMOL Molecular Graphics System, Version 2.0 Schrödinger, LLC
61. Uchihara T (2007) Silver diagnosis in neuropathology: principles, practice and revised interpretation. Acta Neuropathol 113:483–499
62. Wang L, Benzinger TL, Su Y, Christensen J, Friedrichsen K, Aldea P et al (2016) Evaluation of tau imaging in staging Alzheimer disease and revealing interactions between β-amyloid and tauopathy. JAMA Neurol 73:1070–1077
63. Wen GY, Wisniewski HM, Kascsak RJ (1999) Biondi ring tangles in the choroid plexus of Alzheimer's disease and normal aging brains: a quantitative study. Brain Res 832:40–46
64. Werner G, Damme M, Schludi M, Gnörich J, Wind K, Fellerer K et al (2020) Loss of TMEM106B potentiates lysosomal and FTLD-like pathology in progranulin-deficient mice. EMBO Rep 21:e50241
65. Westermark GT, Johnson KH, Westermark P (1999) Staining methods for identification of amyloid in tissue. Meth Enzymol 309:3–25
66. Yadati T, Houben T, Bitorina A, Shiri-Sverdlov R (2020) The ins and outs of cathepsins: physiological function and role in disease management. Cells 9:1679
67. Yalcin A, Ceylan M, Bayraktutan OF, Sonkaya AR, Yuce I (2016) Age and gender related prevalence of intracranial calcifications in CT imaging; data from 12,000 healthy subjects. J Chem Neuroanat 78:20–24
68. Yamashita K, Palmer CM, Burnley T, Murshudov GN (2021) Cryo-EM single particle structure refinement and map calculation using *Servalcat*. Acta Crystallogr D 77:1282–1291
69. Zhao W, Fan Y, Zhao Q, Fan Z, Zhao J, Yu W et al (2024) Tracing TMEM106B fibril deposition in aging and Parkinson's disease with dementia brains. Life Med: lnae011
70. Zhao Q, Fan Y, Zhao W, Ni Y, Tao Y, Bian J et al (2024) A tau PET tracer PBB3 binds to TMEM106B amyloid fibril in brain. Cell Discov 10:50
71. Zhuo X, Brooks M, Jiang P, Koga S, Zuberi AR, Baker MC et al (2020) Loss of Tmem106b exacerbates FTLD pathologies and causes motor deficits in progranulin-deficient mice. EMBO Rep 21:e50197
72. Zivanov J, Nakane T, Forsberg BO, Kimanius D, Hagen WJ, Lindahl E et al (2018) New tools for automated high-resolution cryo-EM structure determination in RELION-3. Elife 7:e42166
73. Zivanov J, Otón J, Ke Z, von Kügelen E, Pyle E, Qu K et al (2022) A Bayesian approach to single-particle electron-tomography in RELION-4.0. Elife 11:e83724